Magnetosome-like ferrimagnetic iron oxide nanocubes for highly sensitive MRI of single cells and transplanted pancreatic islets

Nohyun Lee[a,1], Hyoungsu Kim[b,1], Seung Hong Choi[b], Mihyun Park[a], Dokyoon Kim[a], Hyo-Cheol Kim[b], Yoonseok Choi[b], Shunmei Lin[b], Byung Hyo Kim[a], Hye Seung Jung[c], Hyeonjin Kim[b,d], Kyong Soo Park[c], Woo Kyung Moon[b,2], and Taeghwan Hyeon[a,2]

[a]National Creative Research Initiative Center for Oxide Nanocrystalline Materials, World Class University Program of Chemical Convergence for Energy and Environment, and School of Chemical and Biological Engineering, Seoul National University, Seoul 151-744, Korea; [b]Diagnostic Radiology, Seoul National University Hospital, and the Institute of Radiation Medicine, Medical Research Center, Seoul National University, 28 Yeongeon-dong, Jongno-gu, Seoul 110-744, Korea; [c]Department of Internal Medicine, Seoul National University College of Medicine, 28 Yeongeon-dong, Jongno-gu, Seoul 110-744, Korea; and [d]Lee Gil Ya Cancer and Diabetes Institute, Gachon University of Medicine and Science, Incheon 406-840, Korea

Edited by Nicholas J. Turro, Columbia University, New York, NY 10027, and approved January 3, 2011 (received for review November 5, 2010)

For ultrasensitive magnetic resonance imaging (MRI), magnetic nanoparticles with extremely high r2 relaxivity are strongly desired. Magnetosome-like nanoparticles were prepared by coating polyethylene glycol-phospholipid (PEG-phospholipid) onto ferrimagnetic iron oxide nanocubes (FIONs). FIONs exhibited a very high relaxivity (r2) of 324 mM^{-1} s^{-1}, allowing efficient labeling of various kinds of cells. The magnetic resonance (MR) imaging of single cells labeled with FIONs is demonstrated not only in vitro but also in vivo. Pancreatic islet grafts and their rejection could be imaged using FIONs on a 1.5 T clinical MRI scanner. The strong contrast effect of FIONs enabled MR imaging of transplanted islets in small rodents as well as in large animals. Therefore, we expect that MR imaging of pancreatic islet grafts using FIONs has the potentials for clinical applications. Furthermore, FIONs will enable highly sensitive noninvasive assessment after cell transplantation.

cell tracking | contrast agent | molecular imaging | diabetes | islet transplantation

Nanostructured materials have been studied as novel imaging, diagnostic, and therapeutic agents due to their unique properties (1–3). Magnetic nanoparticles have attracted tremendous attention due to their various biomedical applications (4–7). In particular, superparamagnetic iron oxide nanoparticles (SPIOs) such as Feridex and Resovist have been used as T2 MRI contrast agents due to their ability to shorten T2 relaxation times in the liver, spleen, and bone marrow, by selective uptake and accumulation in the cells of the reticuloendothelial system (8). However, SPIOs generally have relatively low r2 relaxivities because they are synthesized in aqueous media and consequently have poor crystallinity. For ultrasensitive magnetic resonance (MR) imaging, further improvement of r2 relaxivity is strongly desired. Because r2 relaxivity is directly dependent on the magnetic properties of the nanoparticles, there have been several attempts to improve magnetic properties and consequently increase relaxivities by controlling the composition (9, 10), aggregation (11), and oxidation state (12) of magnetic nanoparticles. For clinical utilization, the nanoparticles should be free from toxic transition metal ions such as Co and Mn, because these ions are able to induce harmful effects after degradation and subsequent leaching (13). Recently, MR imaging of single cells was reported using micrometer-sized iron oxide particles (MPIOs), which are micrometer-sized aggregates of SPIOs (14). Because the r2 relaxivity of MPIOs is slightly higher than that of Feridex (15), a large amount of iron still needs to be internalized for the MR imaging of single cells.

Most magnetosomes of magnetotactic bacteria consist of uniform-sized ferrimagnetic iron oxide (magnetite, Fe_3O_4) crystals (16). Interestingly, the size of magnetite crystals in magnetosomes is typically 40–120 nm, which is within the permanent, single-magnetic domain size range with the highest magnetic moment (17). These magnetosomes have considerable potential for various biomedical applications due to their narrow size and shape distribution, high magnetization and inherent biocompatibility (18, 19). Very recently, uniform ferrimagnetic iron oxide (magnetite) nanocubes (FIONs) with sizes ranging from 20–120 nm were produced in multigram scale using a colloidal chemical synthetic route (20). Herein, we report that magnetosome-like polyethylene glycol-phospholipid (PEG-phospholipid)-encapsulated magnetite nanocubes can be used as highly sensitive MR contrast agents for cell tracking and imaging of single cells both in vitro and in vivo. Furthermore we demonstrate that transplanted islets and their immune rejection can be readily imaged using a clinical 1.5 T MR scanner.

Results

Development of FIONs as MR Contrast Agent. Ferrimagnetic iron oxide nanocubes were synthesized via thermal decomposition of iron (III) acetylacetonate in a mixture composed of oleic acid and benzyl ether (20). The resulting magnetite nanoparticles were hydrophobic due to their passivation by oleic acid on the surface. Encapsulation process was employed to transform the as-synthesized hydrophobic nanoparticles to hydrophilic and biocompatible nanoparticles because the process is simple and rapid and consequently prevents extensive agglomeration (21). The encapsulation process was performed simply by adding water into a mixture composed of the hydrophobic FIONs and PEG-phospholipid followed by sonication. The size of the PEG-phospholipid-encapsulated ferrimagnetic iron oxide nanocubes, designated as "FIONs" was 57.8 ± 9.9 nm (Fig. 1*A*). Magnetization of FIONs and Feridex at 300 K was measured to be 132.1 and 64.4 emu per gram of Fe, respectively (Fig. 1*B*). The r2 relaxivities of FIONs, Feridex, and MPIOs dispersed in 1% agarose solution were measured with a 1.5 T clinical MR scanner. At the same iron concentration, FIONs showed the most intense MR contrast effect

Author contributions: N.L., Hyoungsu Kim, W.K.M., and T.H. designed research; N.L., Hyoungsu Kim, S.H.C., M.P., D.K., H.-C.K., Y.S.C., S.L., and B.H.K. performed research; N.L., S.H.C., H.S.J., Hyeonjin Kim, and K.S.P. analyzed data; and N.L., Hyoungsu Kim, W.K.M., and T.H. wrote the paper.

The authors declare no conflict of interest.

This article is a PNAS Direct Submission.

Freely available online through the PNAS open access option.

[1]N.L. and Hyoungsu Kim contributed equally to this work.

[2]To whom correspondence may be addressed. E-mail: thyeon@snu.ac.kr or moonwk@radcom.snu.ac.kr.

This article contains supporting information online at www.pnas.org/lookup/suppl/doi:10.1073/pnas.1016409108/-/DCSupplemental.

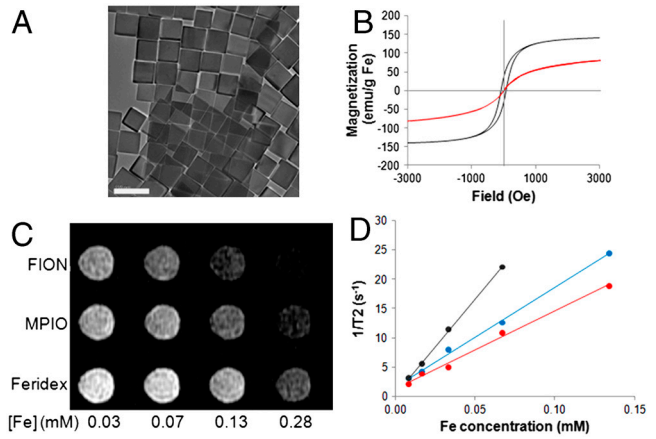

Fig. 1. TEM image, magnetic properties, and MR images of ferrimagnetic iron oxide nanoparticles (FION). (*A*) TEM image of FIONs. The size of FIONs was 57.8 ± 9.9 nm and their shape was cubic. Scale bar, 100 nm. (*B*) The M-H curve of FION (black) and Feridex (red). The saturation magnetization of FIONs was 132.1 emu/g Fe, which is twice as high as that of Feridex (64.4 emu/g Fe). (*C*) T2 weighted MR image of FION, MPIO and Feridex at various concentrations of iron. (*D*) Plots of R2 value of FION ($r2 = 324\ mM^{-1}\ s^{-1}$, black), MPIO ($r2 = 169\ mM^{-1}\ s^{-1}$, blue), and Feridex ($r2 = 133\ mM^{-1}\ s^{-1}$, red). FIONs have much higher magnetization and show stronger T2 contrast effect than MPIO and Feridex.

(Fig. 1*C*). The r2 of FIONs was measured to be 324 $mM^{-1}\ s^{-1}$, which is much higher than that of Feridex or MPIOs (Fig. 1*D*). It is also noteworthy that the r2 of FIONs per particle was 2 or 3 orders of magnitude higher than that of previously reported superparamagnetic nanoparticles (Table S1) (12).

MR Imaging of Single Cells. MDA-MB-231 human breast cancer cells were labeled by the addition of FIONs to the culture medium at a concentration of 25 μg Fe/mL, followed by incubating overnight. Free FIONs were removed using Ficoll–Paque, which is often used for purification of viable cells from blood samples based on density difference. Prussian blue staining of the labeled cells revealed that FIONs were efficiently taken up without any extra treatment to enhance cellular uptake (Fig. 2*A*). To confirm the internalization of FIONs, the labeled cells were detached by trypsin treatment. The image of the detached cells clearly shows that the particles were not on the cell surface, but instead located inside the cells (Fig. 2*B*). The transmission electron microscope (TEM) image of the labeled cells shows that the endocytosed FIONs were found in vesicles such as endosomes and lysosomes (Fig. 2*C*). Although the exact mechanism of the uptake of FIONs needs to be elucidated, sedimentation of the nanoparticles seems to have increased the chance for contact with the cells during incubation. FIONs were also readily taken up by a suspension cell line (K562, human leukemia cell), but the uptake amount was smaller than that of the monolayer cell lines, probably because the chance of contact with the cells was limited once sedimentation occured (Fig. S1). During incubation of the cells with FIONs, no deleterious effect such as change in cell morphology was observed. The cytotoxicity of FIONs was evaluated using MTT (3-(4,5-Dimethylthiazol-2-yl)-2,5-Diphenyltetrazolium Bromide) and trypan blue assays, and no appreciable toxicity was observed (Fig. S2).

To image the single cells labeled with FIONs, a high-resolution 9.4 T MR scanner was employed. The cells were simultaneously labeled with fluorescent calcein-AM after their incubation with FIONs to correlate the MR images with the fluorescence images. Subsequently, several labeled cells were carefully picked up and sandwiched between two 1% Gelrite layers. Although the size of the cells is smaller than the resolution of the MRI (100 μm), the strong blooming effect of FIONs enabled MR imaging of single

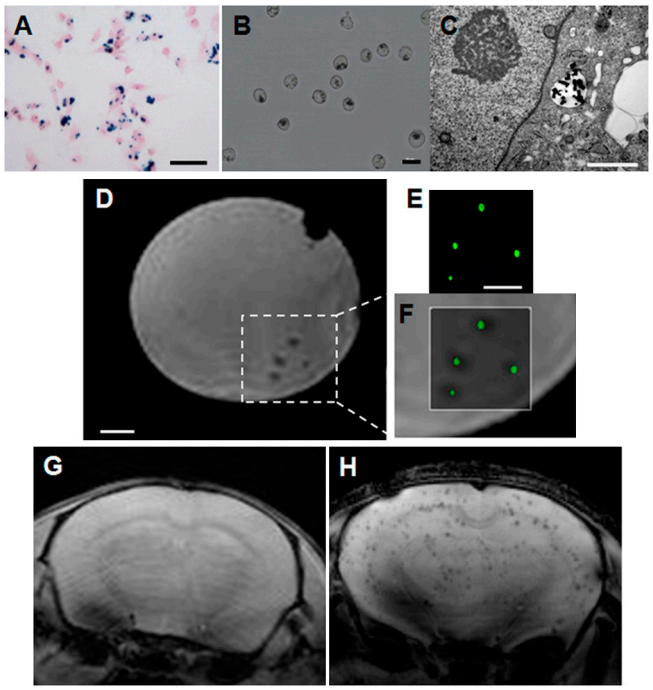

Fig. 2. Cellular uptake of FIONs and MR images of single cells. (*A*) Prussian blue stains of MDA-MB-231 breast cancer cells. (*B*) Trypsinized MDA-MB-231 cells. The FIONs are visible as dark spots inside the cells. (*C*) TEM image of FIONs trapped in the vesicle of cells. Cells were labeled for 24 hr at 25 μg Fe/mL. (*D*) MR image of four labeled cells sandwiched between two Gelrite layers. (*E*) Fluorescence image of cells stained with calcein-AM. (*F*) Merged image of corresponding region of (*D*) and (*E*). The dark spots in MR image matched exactly with green spots in fluorescence image. (*G* and *H*) In vivo T2* MR images of brain of control mouse that received no cells (*G*) and mouse that received intracardiac injection of 1×10^6 of FION-labeled cells (*H*). The injected cells were entrapped in the capillaries and appeared as dark spots in MR image. Scale bars, 20 μm (*A* and *B*); 1 μm (*C*); 1 mm (*D* and *E*).

cells. Several dark spots could be observed in the T2* MR images (Fig. 2*D*). These dark spots matched exactly with the green spots in the fluorescence image of the corresponding region (Fig. 2 *E* and *F*). The merged MR and fluorescence image clearly shows that the single cells labeled with FIONs were readily detected by MRI. On the other hand, the cells labeled with Feridex-poly-*l*-lysine (PLL) showed very weak contrast effect under identical imaging conditions (Fig. S1*D* and Fig. S3).

To demonstrate in vivo MR imaging of single cells, MDA-MB-231 cells were labeled with FIONs, and 1×10^6 cells were carefully injected into the left ventricle of a mouse heart. The intracardially injected cells were delivered to various organs by arterial circulation and entrapped in the capillaries. MR imaging of the mouse brain was performed with a 9.4 T MR scanner 1 hr after the injection of labeled cells. The retained cells in the mouse brain were revealed as multiple dark spots in the T2* MR images, whereas no dark spot was observed in the MR images of the untreated mouse (Fig. 2 *G* and *H*). The Prussian blue stained image of the mouse brain sections shows the presence of a solitary iron-positive cell (Fig. S4). Although a direct comparison of the MR images and Prussian blue staining images is difficult due to a difference in image thickness (the thickenesses of MR images and stained images were 1 mm and 8 μm, respectively), aggregates of multiple iron-positive cells were not found by histological observation. This means that the dark spots in the MR images of the brain were due to solitary single cells labeled with FIONs. This high sensitivity of FIONs makes them an ideal T2 contrast agent for the MR imaging of cellular events.

In Vitro Labeling of Pancreatic Islets with FIONs. After FIONs were confirmed to have high sensitivity in MR imaging, the feasibility of MR imaging of pancreatic islets using a clinical 1.5 T MR scanner was evaluated. To test whether or not FIONs could be taken up, the rat pancreatic islets were isolated and incubated with FIONs for 6 hr at a concentration of 50 μg Fe/mL. Due to their ferrimagnetic property, FIONs aggregated and were revealed as dark spots in pancreatic islets using a light microscope (Fig. 3*A*). FIONs localized mostly to peripheral cells of the islets because they could not diffuse into the center of the islets (Fig. 3*B*). To confirm that FIONs were internalized by the cells, and not simply adherent to the cell surfaces, the labeled islets were observed by TEM. The TEM image shows that FIONs were located inside the cells (Fig. 3*C*). Uptake of FIONs was so rapid that a single islet could be observed using a clinical 1.5 T MR scanner as early as 2 hr after the incubation (Fig. S5). The MTT test shows that the viability of labeled islets did not vary significantly compared to the unlabeled islets (Fig. 3*D*). Because the number of cells that contained FIONs was relatively small, the influence of FIONs on cell viability was further evaluated using calcein AM/PI staining. The viability of control islets, islets incubated with 25 μg Fe/mL, and islets incubated with 50 μg Fe/mL was $95.7 \pm 2.3\%$, $93.5 \pm 2.8\%$, and $97.4 \pm 3.9\%$, respectively (Fig. 3*E*), demonstrating that the cells internalized with FIONs were viable after the labeling. The function of islets was assessed by a glucose stimulated insulin secretion test. The stimulation indices (ratio of stimulated over basal insulin secretion) were 3.01 ± 0.43, 3.29 ± 0.10, and 3.05 ± 0.35 for control islets, islets incubated with 25 μg Fe/mL, and islets incubated with 50 μg Fe/mL, respectively (Fig. 3 *F* and *G*).

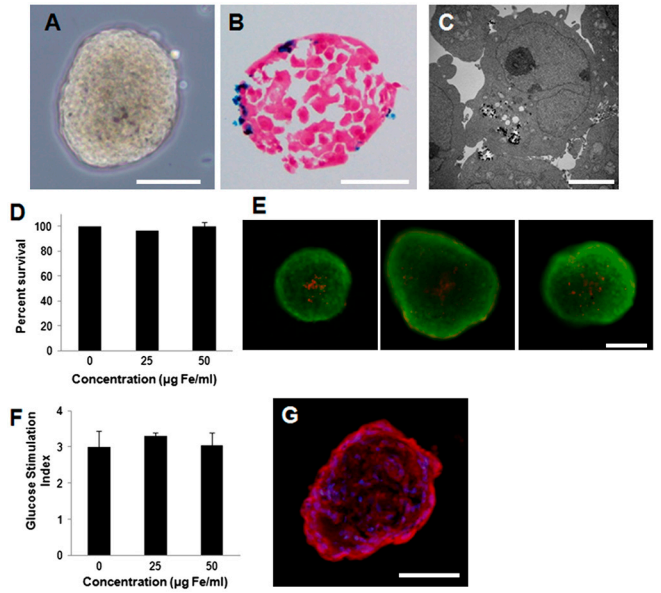

Fig. 3. Labeling of pancreatic islets with FIONs. (*A*) Live rat pancreatic islet labeled with FIONs. The internalized FIONs are visible as dark spot in islet. (*B*) Prussian blue stain of frozen section of labeled islet. Internalized FIONs were stained as blue and nuclei were counterstained with nuclear fast red. (*C*) TEM image of labeled islets. The pancreatic islets were labeled by incubation with FION for 6 hr at 25 μg Fe/mL. (*D* and *E*) Viability of islets labeled with FIONs. (*D*) Percentage survival of labeled islet 24 hr after incubation with FION ($n = 4$ for each group, $P > 0.05$). (*E*) Live cells and dead cells were stained with Calcein-AM (green) and propidum iodide (red), respectively 24 hr after FION incubation. The viability of control islet (*Left*), islet incubated at 25 μg Fe/mL (*Center*) and islet incubated at 50 μg Fe/mL (*Right*) was $95.7 \pm 2.3\%$, $93.5 \pm 2.8\%$, and $97.4 \pm 3.9\%$, respectively ($P > 0.05$). (*F* and *G*) Functionality of islets labeled with FIONs. (*F*) Glucose stimulation indices (ratio of secreted insulin level at high glucose over basal insulin release) of control islets, islets incubated at 25 μg Fe/mL and islets incubated at 50 μg Fe/mL were 3.01 ± 0.43, 3.29 ± 0.10, and 3.05 ± 0.35, respectively ($n = 4$ for each group, $P > 0.05$). (*G*) Fluorescence image of frozen section of labeled islet. Insulin producing β-cells were stained as red. The nuclei were stained with DAPI (blue). Scale bars, 80 μm (*A*, *B*, *E*. and *G*); 4 μm (*C*). Error bars are SD.

In Vivo MR Imaging of Transplanted Syngeneic Islets. To assess the feasibility of in vivo MR imaging of islets transplanted into the liver, syngeneic islets labeled with FIONs were intraportally infused into streptozotocin-induced diabetic F344 rats ($n = 4$). After transplantation, the rats became euglycemic (blood glucose level ~100 mg/dl), and no relapse of diabetes was observed (Fig. S6*A*). In contrast, the rats that did not receive islet transplantation remained hyperglycemic (blood glucose level ~400 mg/dl). This indicates that the decreased blood glucose level resulted from the transplantation of islets rather than restoration of residual islet function in the recipient rats. Intraperitoneal glucose tolerance test showed that the change in glucose level of transplanted rats was similar to that of normal rats, whereas untreated diabetic rats showed large changes in their blood glucose levels (Fig. S6*B*). In vivo MR imaging was performed by a clinical 1.5 T scanner up to 150 d to follow up on the fate of transplanted islets. After infusion, the islets were clearly observed as dark spots within the liver in the T2* MR images (Fig. 4 *A–F*). The islets were distributed preferentially in the liver peripheral region according to portal vein flow. The ex vivo MR image and microscope image of a corresponding liver section stained with Prussian blue show tha the dark spots indicate single islets and/or islet clusters (Fig. S7). The dark spots were observed for up to 150 d, and the number of spots decreased slowly (Fig. S8*A*). Sections of liver showed that islets were not destroyed by host immune attack and that FIONs were retained in syngeneic islets (Fig. 4 *G* and *H*).

In Vivo MR Imaging of Immune Rejection of Transplanted Allogeneic Islets. To image immune rejection, islets from F344 rats were infused into the liver of Sprague–Dawley (SD) rats ($n = 4$). In this study, diabetes was not induced to avoid the harmful effect of glucose on the islets. The number of dark hypointense spots in the T2* MR images rapidly decreased after transplantation (Fig. 5 *A–F* and Fig. S8*B*). This decrease resulted from allograft

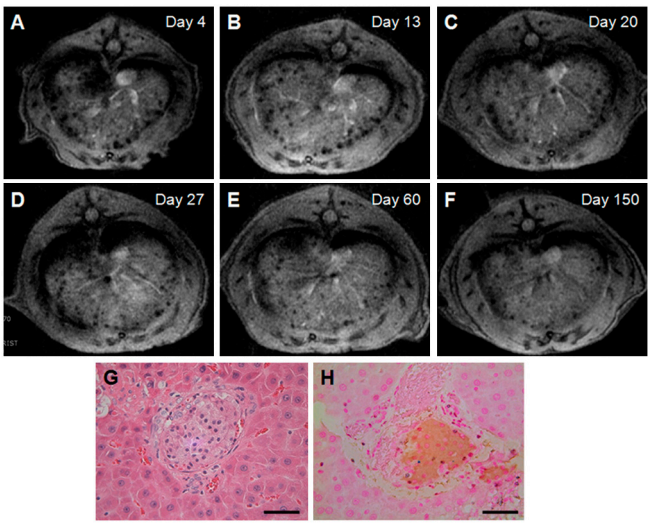

Fig. 4. In vivo MR images of intrahepatically transplanted syngeneic islets. (*A–F*) T2* MR images of rat liver infused with ~3,000 pancreatic islets; 4 d (*A*), 13 d (*B*), 20 d (*C*), 27 d (*D*), 60 d (*E*), and 150 d (*F*) after transplantation. The hypointense spots representing labeled islet persisted up to 150 d after transplantation. (*G* and *H*) Histological examination of liver after syngeneic islet transplantation. (*G*) *H* and *E* stain shows normal structure of pancreatic islets in liver. (*H*) Immunohistochemistry shows the presence of FIONs (Prussian blue stain, blue) in islet β cells (insulin, brown). Scale bars, 50 μm (*G* and *H*).

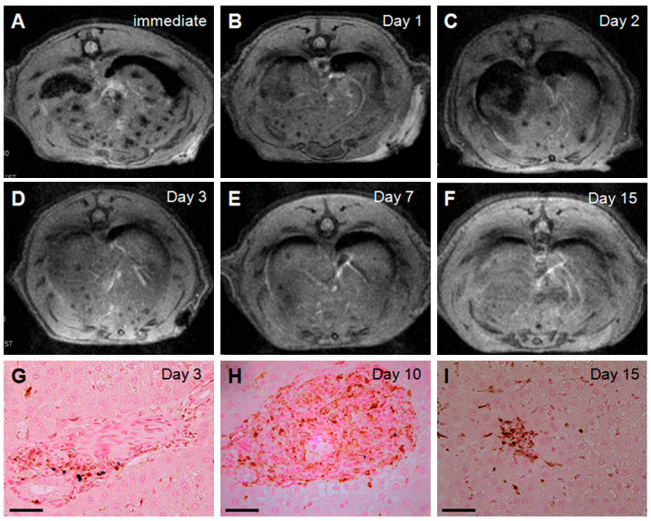

Fig. 5. In vivo MR images of intrahepatically transplanted allogeneic islets. (*A–F*) T2* MR images of rat liver infused with allogeneic islets; immediately (*A*), 1 d (*B*), 2 d (*C*), 3 d (*D*), 7 d (*E*), and 15 d (*F*) after transplantation. In contrast to syngeneic islets, the number of hypotintense spots representing labeled islets decreased. (*G–I*) Histological examination of liver; 3 d (*G*), 10 d (*H*), and 15 d (*I*) after allogeneic islet transplantation. The macrophages (CD 68, brown) invaded allogeneic islets and accumulated. FIONs were released during immune rejection. The released FIONs were not found after 14 d indicating their clearance by liver parenchyma. Scale bars, 50 μm (*G–I*).

rejection rather than mechanical injury and ischemia during the transplantation. Immunohistochemical observation revealed the infiltration of macrophages into the islets (Fig. 5 *G–I*). The infiltration became more severe and the volume of the islets decreased with time. The fate of FIONs was also traced using Prussian blue staining. Until 3 d after tranplantation, iron was observed in the islets (Fig. 5*G*). FIONs seemed to be released from the islets after cell death because they were not observed in islets 10 d after transplantation (Fig. 5*H*). Clearance of the released FIONs was so rapid that only a trace amount of iron was observed 14 d after transplantation (Fig. 5*I*).

In Vivo MR Imaging of Islet Transplantation in a Swine Model. The feasibility of MR imaging of transplanted islets in a clinical situation was assessed by in vivo imaging of islet engraftment in a swine model. Because swine islets are rapidly destroyed during transplantation (22), the recipient swine was treated with immunosuppressive drugs (23). The transplantation was then performed by an interventional radiologist (24). A percutaneous transhepatic approach was used to gain access to the portal vein. Ultrasonography and fluoroscopy were used to determine the point of hepatic puncture and catheter placement into the portal vein. The islets were slowly administered by gravity force to reduce damage from shear stress. After the infusion, islets were observed in the T2* MR images as hypointense spots throughout the liver (Fig. 6 *A* and *B*). On the contrary, no dark spot was shown in swine that did not receive immunosuppressive treatment (Fig. 6*C*). These results demonstrate that islet engraftment can be monitored using FIONs even in large animals.

Discussion

FIONs and magnetosomes are very similar in size, shape, and surface coating. We were able to fabricate a highly sensitive MR contrast agent by using ferrimagnetic magnetite nanocrystals with single-magnetic domain size and biocompatible PEG-phospholipid coating. Because the magnetization of FIONs is much higher than that of SPIO, the r2 relaxivity of FIONs was 2 or 3 times higher as well (Fig. 1). The nanocrystals were made of iron oxide and free from toxic elements. Because iron oxide is

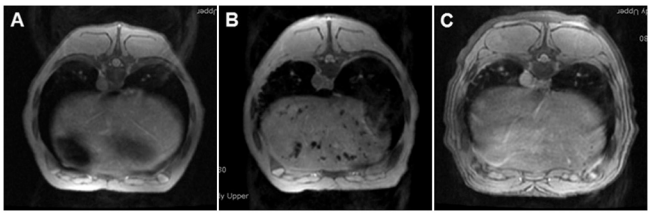

Fig. 6. In vivo MR images of intrahepatically transplanted islets in swine models. (*A* and *B*) T2* MR images of immunosuppressed swine liver infused with allogeneic islets; prior to transplantation (*A*), and after transplantation (*B*). Transplanted islets were shown as hypointense spots. The transplanted islets that were not attacked by host immune system diffused throughout the liver. (*C*) T2* MR image of nonimmunosuppressed swine liver after islet tranplantation. Few hypointense spots were shown, which indicates the tranplanted islets were immediately damaged.

in the fully oxidized state of iron, the chemical and magnetic properties of FIONs do not change for a long time. Furthermore, degradation and subsequent clearance of FIONs by liver parenchyma was observed after destruction of the infused islets (Fig. 5*I*). Previous reports also showed that iron oxide nanoparticles were metabolized and that iron was incorporated into the body's iron store (25).

MRI has been intensively studied for the tracking of labeled cells (26). To precisely investigate cell-level events, it is highly desirable to have the ability to image a very small number or single cells. To improve the cellular MRI capability, there have been various attempts to increase the cellular uptake of nanoparticles, such as conjugation with cell-penetrating peptides (27), encapsulation with dendrimers (28), and coincubation with transfection agents such as PLL (29). However, these approaches involve complicated conjugation steps, which sometimes lead to cell death by generating transient holes in the cell membrane (30). In this study, the cells could be easily labeled with FIONs without any treatment to increase cellular uptake (Fig. 2*A*). FIONs did not affect the viability or function of the labeled cells. The TEM image of the labeled cells showed that the FIONs were confined in the endosomes after the internalization (Fig. 2*C*). Consequently the function of cells did not seem to be affected by the strong magnetic field of MR scanner during the imaging. For example, insulin secretion of the labeled islets was similar to the unlabeled ones (Fig. 3*F*), and diabetic rats became euglycemic after the islet transplantation and subsequent repetitive MR imaging (Fig. S6).

Both high relaxivity and large uptake amount seemed to enable the MR imaging of single cells. The uptake amount of FIONs into cells was much larger compared to Feridex (SPIO) coincubated with transfection agent, PLL. However, the uptake amount of FIONs was smaller than Feridex when the pancreatic islets were incubated with the nanoparticles. The reduced internalization of FIONs into the islets was due to their ferrimagentic property. Because FIONs rapidly aggregated, they were not able to easily diffuse into the interior of the islets (Fig. 3*B*). By contrast, SPIOs are well-dispersible and readily diffuse into the islets (31). The large magnetization and resulting high relaxivity of FIONs enabled the MR imaging of islets using a clinical 1.5 T MR scanner. The relaxivity and uptake amount of magnetic nanoparticles should be finely controlled for the successful imaging of transplanted islets and their immune rejection. The islets are unable to be imaged if their relaxivity or uptake amount is too low. In contrast, excessively high relaxivity and too much uptake may delay the detection of loss of islets because the local magnetization and concentration around islet grafts after immune cell infiltration may remain high.

According to previous reports, overnight incubation was required to label the islets with Feridex, and the minimum detectable number of islets using a clinical 1.5 T MR scanner was ~200

in vivo (32). For this reason, a high tesla animal MR scanner, which is not clinically available, was employed in most of the previous reports (31). In the current report, however, single islets were able to be observed as early as 2 hr after incubation with FIONs using a clinical 1.5 T MR scanner (Fig. S5). Because the vasculatures of pancreatic islets are disrupted during isolation, the short labeling time is desirable for improving the viability and functionality of transplanted islets (33). The syngeneic islets transplanted into the liver were able to be observed up to 150 d after transplantation, although the number and size of their hypointense spots in the T2* images slowly decreased (Fig. 4).

The decrease in the number of hypointense spots of the allografted islets was rapid (Fig. 5). Previous reports show that the median survival time of allotransplanted islets in rats was 7 d (34). In this report, the number of dark spots representing allografted islets decreased significantly, even 1 d after transplantation. Furthermore, immunohistochemical sections of liver 3 d after transplantation showed that the infiltration of immune cells had already begun (Fig. 5*G*). Therefore, it appeared that FIONs in the islets were released as soon as the immune cells infiltrated, showing that the decrease in the number of hypointense spots indicated the start of immune rejection.

MR imaging of transplanted islets in humans was turned out to be extremely challenging (35), and novel contrast agents or imaging methods are required to image transplanted islets in humans (36). Imaging of a large animal requires a large field of view (FOV), which inevitably results in low resolution and reduced signal-to-noise ratio. Although the T2 and T2* contrast effects are enhanced at a high magnetic field of >3 T, it is unclear whether or not high tesla MRI can be used clinically due to saftey issues. Barnett et al. showed successful imaging of intrahepatically transplanted islets, which were protected by magneto-capsules, in a swine model at 1.5 T (37). Although the alginate capsule protects the islets from host immune attack, it also hinders the diffusion of oxygen and nutrients (33). Furthermore, loss of graft function or islets is very difficult to detect with MR imaging unless the alginate capsules are ruptured. In this report, the transplanted islets in a large animal were readily observed using a clinical MR scanner (Fig. 6). FIONs could find their clinical applications such as highly sensitive noninvasive assessment of transplanted cells because the amount of incorporated FIONs is very small and the chemical composition of FIONs is the same as Feridex, which is a clinically approved MRI contrast agent.

In conclusion, magnetosome-like PEG-phospholipid-stabilized FIONs were developed for the MR imaging of single cells and transplanted pancreatic islets. FIONs exhibited a very high relaxivity and were able to label various kinds of cells efficiently. Whereas their low colloidal stability limits their in vivo applications that require long circulation time, they enable highly sensitive MR imaging of ex vivo labeled cells. Herein, the MR imaging of single cells at high tesla MRI and pancreatic islets at clinical MRI was demonstrated. We expect that FIONs have enormous potentials not only for fundamental biomedical research but also for clinical cell therapy.

Materials and Methods

A detailed description of materials and methods is available in *SI Materials and Methods*.

Preparation of FIONs. Ferrimagnetic iron oxide nanocubes were synthesized according to the previous report (20). To render the nanoparticle hydrophilic, 2 mL of the organic dispersible ferrimagnetic iron oxide nanocubes in chloroform (5 mg/mL) was mixed with 1 mL of chloroform containing 10 mg of 1, 2-distearoyl-sn-glycero-3-phosphoethanolamine-N-[methoxy(polyethylene glycol)-2000] (PEG-phospholipid, Avanti Polar Lipids, Inc.). After evaporating the solvent, the resulting mixture was incubated at 80 °C under vacuum for 1 hr. Subsequently 2 mL of sterilized water was added and sonicated to disperse FIONs. Excess PEG-phospholipid was removed by centrifugation.

In Vivo and in Vitro MR Imaging of Single Cells. The cells were magnetically labeled with FION or Feridex-PLL (as described in *SI Materials and Methods*). Subsequently, the cells were fluorescently labeled with calcein-AM (Fluka). The cells were then incubated with 10 μM of freshly prepared calcein-AM solution for 30 min. A few cells were picked up using a micropipette and sandwiched between 1% Gelrite layers. MR imaging was performed using a rat head coil on a 9.4 T MRI scanner (Bruker, BioSpec 94/20). The gradient T_2* images were acquired using the following measurement parameters: flip angle = 90°, TR = 5,000 ms, TE = 13.1 ms, NEX = 4, FOV = 2.5 cm × 2.5 cm, matrix = 256 × 256, thickness = 0.5 mm.

In vivo mouse experiments were approved by the Institutional Animal Care and Use Committee of Gachon University. Balb/c nude mice weighing 25 g were used for in vivo MR imaging. 1×10^6 MDA-MB-231 cells labeled with FIONs were dispersed in free DMEM and injected into the left ventricle of heart. One hr after injection, MR imaging was performed using a rat head coil on a 9.4 T MRI scanner. The gradient T2* images were acquired using the following measurement parameters: flip angle = 90°, TR = 5,000 ms, TE = 7.6 ms, NEX = 1, FOV = 2.0 cm × 2.0 cm, matrix = 256 × 256, thickness = 1 mm.

Labeling of Rat Islets. This experiment was approved by the Institutional Animal Care and Use Committee (IACUC) of the Clinical Research Institute of Seoul National University Hospital. Pancreatic islets were isolated from Fischer 344 (F344) rats. After intraductal collagenase P (Roche Applied Science) injection, the pancreas was removed and digested for 15 min at 37 °C. After washing with Hanks' balanced salt solution (HBSS, Sigma), the pancreatic islets were purified by centrifugation in a discontinuous Ficoll (GE Healthcare) gradient. The purified islets were labeled by incubation in Roswell Park Memorial Institute 1640 medium (RPMI medium 1640) containing FIONs (50 μg Fe/mL) for 12 hr. After labeling, free FIONs were removed by centrifugation in discontinuous Ficoll gradient.

In Vitro and in Vivo MR Imaging of Rat Islets. For in vitro MR imaging, labeled islets were sandwiched between Gelrite layers in ELISA plate as described above. In vitro phantom MRI was performed using a 4-channel wrist coil on a clinical 1.5 T MRI scanner. 3D gradient echo (GRE) images were acquired using the following parameters: flip angle = 10°, TR = 58 ms, TE = 12 ms, NEX = 2, FOV = 8.0 cm × 8.0 cm, matrix = 256 × 256, thickness = 0.7 mm.

For in vivo MR imaging, ~3,000 labeled islets per recipient were infused into the portal vein of streptozotocin-induced diabetic F344 rats (syngeneic graft model) or healthy Sprague–Dawley (SD) rats (allogeneic graft model). After transplantation, MR imaging was performed using a 4-channel wrist coil on a clinical 1.5 T MRI scanner. The T2* multigradient echo (MGRE) images were acquired using the following parameters: flip angle = 20°, TR = 800 ms, TE = 15 ms, NEX = 2, FOV = 7.0 cm × 7.0 cm, matrix = 256× 192, thickness = 2 mm. The number of dark signal intensity voxels in rat livers was measured by Image J program.

Swine Studies. This experiment was approved by the IACUC of the Clinical Research Institute of Seoul National University. Pig islets were isolated from adult market pigs according to a previous report (38). After isolation, the islets were incubated in Medium 199 supplemented with 10% pig serum at 37 °C. The purified islets were labeled by incubation in medium containing FIONs (50 μg Fe/mL) for 12 hr. Immunosuppression was initiated before transplantation. The recipient, a hybrid pig, was orally administered sirolimus (Rapamune, 1 mg) and tacrolimus (Prograf, 1 mg). Transplantation was then performed by an interventional radiologist according to the previous report with a slight modification (24). After transplantation, MR imaging was performed using an 8 channel body coil on a clinical 1.5 T MRI scanner. The T2* MGRE images were acquired using following the measurement parameters: flip angle = 20°, TR = 800 ms, TE = 14.5 ms, NEX = 2, FOV = 28.0 cm × 28.0 cm, matrix = 256 × 192, thickness = 3 mm.

Statistical Analysis. Values are presented as means ± SD. All error bars represent SD. The statistical significance of differences was determined by Student's *t* test.

ACKNOWLEDGMENTS. T.H. acknowledges financial support by the Korean Ministry of Education, Science, and Technology through National Creative Research Initiative (R16-2002-003-01001-0), Strategic Research (2010-0029138), and World Class University (R31-10013) Programs of National Research Foundation (NRF) of Korea. W.K.M. acknowledges financial support from the Innovative Research Institute for Cell Therapy (A062260).

1. Rosi NL, Mirkin CA (2005) Nanostructures in biodiagnostics. *Chem Rev* 105:1547–1562.
2. Medintz IL, Uyeda HT, Goldman ER, Mattoussi H (2005) Quantum dot bioconjugates for imaging, labelling and sensing. *Nat Mater* 4:435–446.
3. Cao YC, Jin R, Mirkin CA (2002) Nanoparticles with Raman spectroscopic fingerprints for DNA and RNA detection. *Science* 297:1536–1540.
4. Gao J, Gu H, Xu B (2009) Multifunctional magnetic nanoparticles: Design, synthesis, and biomedical applications. *Acc Chem Res* 42:1097–1107.
5. Hao R, et al. (2010) Synthesis, functionalization, and biomedical applications of multifunctional magnetic nanoparticles. *Adv Mater* 22:2729–2742.
6. Cheng K, Peng S, Xu C, Sun S (2009) Porous hollow Fe_3O_4 nanoparticles for targeted delivery and controlled release of cisplatin. *J Am Chem Soc* 131:10637–10644.
7. Gao J, et al. (2008) Multifunctional yolk-shell nanoparticles: a potential MRI contrast and anticancer agent. *J Am Chem Soc* 130:11828–11833.
8. Na HB, Song IC, Hyeon T (2009) Inorganic nanoparticles for MRI contrast agents. *Adv Mater* 21:2133–2148.
9. Seo WS, et al. (2006) FeCo/graphitic-shell nanocrystals as advanced magnetic-resonance-imaging and near-infrared agents. *Nat Mater* 5:971–976.
10. Lee J-H, et al. (2007) Artificially engineered magnetic nanoparticles for ultra-sensitive molecular imaging. *Nat Med* 13:95–99.
11. Perez JM, Josephson L, O'Loughlin T, Högemann D, Weissleder R (2002) Magnetic relaxation switches capable of sensing molecular interactions. *Nat Biotechnol* 20:816–820.
12. Lee H, Yoon T-J, Weissleder R (2009) Ultrasensitive detection of bacteria using core-shell nanoparticles and an NMR-filter system. *Angew Chem Int Edit* 48:5657–5660.
13. Limbach LK, et al. (2007) Exposure of engineered nanoparticles to human lung epithelial cells: Influence of chemical composition and catalytic activity on oxidative stress. *Environ Sci Technol* 41:4158–4163.
14. Shapiro EM, et al. (2004) MRI detection of single particles for cellular imaging. *Proc Natl Acad Sci USA* 101:10901–10906.
15. Wu YL, et al. (2006) In situ labeling of immune cells with iron oxide particles: An approach to detect organ rejection by cellular MRI. *Proc Natl Acad Sci USA* 103:1852–1857.
16. Bazylinski DA, Frankel RB (2004) Magnetosome formation in prokaryotes. *Nat Rev Microbiol* 2:217–230.
17. Stolz JF, Chang S-BR, Kirschvink JL (1986) Magnetotactic bacteria and single-domain magnetite in hemipelagic sediments. *Nature* 321:849–851.
18. Staniland S, et al. (2008) Controlled cobalt doping of magnetosomes in vivo. *Nat Nanotehnol* 3:158–162.
19. Mandal D, Bolander ME, Mukhopadhyay D, Sarkar G, Mukherjee P (2006) The use of microorganisms for the formation of metal nanoparticles and their application. *Appl Microbiol Biotechnol* 69:485–492.
20. Kim D, et al. (2009) Synthesis of uniform ferrimagnetic magnetite nanocubes. *J Am Chem Soc* 131:454–455.
21. Dubertret B, et al. (2002) In vivo imaging of quantum dots encapsulated in phospholipid micelles. *Science* 298:1759–1762.
22. Eich T, et al. (2007) Positron emission tomography: A real-time tool to quantify early islet engraftment in a preclinical large animal. *Transplantation* 84:893–898.
23. Echeverri GJ, et al. (2009) Endoscopic gastric submucosal transplantation of islets (ENDO-STI): Technique and initial results in diabetic pigs. *Am J Transplant* 9:2485–2496.
24. Owen RJT, et al. (2003) Percutaneous transhepatic pancreatic islet cell transplantation in type 1 diabetes mellitus: Radiologic aspects. *Radiology* 229:165–170.
25. Bourrinet P, et al. (2006) Preclinical safety and pharmacokinetic profile of Ferumoxtran-10, an ultrasmall superparamagnetic iron oxide magnetic resonance contrast agent. *Invest Radiol* 41:313–324.
26. de Vries IJM, et al. (2005) Magnetic resonance tracking of dendritic cells in melanoma patients for monitoring of cellular therapy. *Nat Biotechnol* 23:1407–1413.
27. Koch AM, et al. (2003) Uptake and metabolism of a dual fluorochrome Tat-nanoparticle in HeLa cells. *Bioconjugate Chem* 14:1115–1121.
28. Bulte JWM, et al. (2001) Magnetodendrimers allow endosomal magnetic labeling and in vivo tracking of stem cells. *Nat Biotechnol* 19:1141–1147.
29. Frank JA, et al. (2003) Clinically applicable labeling of mammalian and stem cells by combining superparamagnetic iron oxides and transfection agents. *Radiology* 228:480–487.
30. Leroueil PR, et al. (2007) Nanoparticle interaction with biological membranes: Does nanotechnology present a Janus face? *Acc Chem Res* 40:335–342.
31. Evgenov NV, Medarova Z, Dai G, Bonner-Weir S, Moore A (2006) In vivo imaging of islet transplantation. *Nat Med* 12:144–148.
32. Tai JH, et al. (2006) Imaging islets labeled with magnetic nanoparticles at 1.5 Tesla. *Diabetes* 55:2931–2938.
33. Narang AS, Mahato R (2006) Biological and biomaterial approaches for improved islet transplantation. *Pharmacol Rev* 58:194–243.
34. Lee DY, Lee S, Nam JH, Byun Y (2006) Minimization of immunosuppressive therapy after islet transplantation: Combined action of heme oxygenase-1 and PEGylation to islet. *Am J Transplant* 6:1820–1828.
35. Toso C, et al. (2008) Clinical magnetic resonance imaging of pancreatic islet grafts after iron nanoparticle labeling. *Am J Transplant* 8:701–706.
36. Medarova Z, Moore A (2009) MRI as a tool to monitor islet transplantation. *Nat Rev Endocrinol* 5:444–452.
37. Barnett BP, et al. (2007) Magnetic resonance-guided, real-time targeted delivery and imaging of magnetocapsules immunoprotecting pancreatic islet cells. *Nat Med* 13:986–991.
38. Kim H-I, et al. (2009) The effect of composite pig islet-human endothelial cell grafts on the instant blood-mediated inflammatory rejection. *Cell Transplant* 18:31–37.